High-efficiency and ultrabroadband flexible absorbers based on transversely symmetrical multi-layer structures

Cite as: AIP Advances **9**, 115007 (2019); https://doi.org/10.1063/1.5119406
Submitted: 11 July 2019 . Accepted: 26 October 2019 . Published Online: 14 November 2019

Jing Ma, Jicheng Wang, Zheng-Da Hu, Zhidong Zhang, Liang Pan, and Andrea Di Falco

High-efficiency and ultrabroadband flexible absorbers based on transversely symmetrical multi-layer structures

Cite as: AIP Advances 9, 115007 (2019); doi: 10.1063/1.5119406
Submitted: 11 July 2019 • Accepted: 26 October 2019 •
Published Online: 14 November 2019

Jing Ma,[1,2] Jicheng Wang,[1,a)] Zheng-Da Hu,[1] Zhidong Zhang,[3] Liang Pan,[4] and Andrea Di Falco[2,a)]

AFFILIATIONS

[1]School of Science, Jiangsu Provincial Research Center of Light Industrial Optoelectronic Engineering and Technology, Jiangnan University, Wuxi 214122, China
[2]School of Physics and Astronomy, University of St Andrews, St Andrews KY16 9SS, United Kingdom
[3]Science and Technology on Electronic Test and Measurement Laboratory, North University of China, Taiyuan 030051, China
[4]School of Mechanical Engineering and Birck Nanotechnology Center, Purdue University, West Lafayette, Indiana 47907, USA

[a)]**Authors to whom correspondence should be addressed:** jcwang@jiangnan.edu.cn and adf10@st-andrews.ac.uk

ABSTRACT

Two ultrabroadband and omnidirectional perfect absorbers based on transversely symmetrical multilayer structures are presented, which are achieved by four absorptive metal chromium (Cr) layers, antireflection coatings, and the substrates, glass and PMMA, in the middle. At the initial step, the proposed planar structure shows an average absorption of ~93% over the visible (VIS) and near-infrared range from 400 to 2500 nm and 98% in the VIS range. The optimum flat is optically characterized by the transfer matrix method and local metal-insulator-metal resonance under illumination with transverse-electric and transverse-magnetic polarization waves. The multilayer materials, which are deposited on an intermediate substrate by e-beam evaporation, outperform the previously reported absorbers in the fabrication process and exhibit a great angular tolerance of up to 60°. Afterward, we present a novel symmetrical flexible absorber with the PMMA substrate, which shows not only perfect absorption but also the effect of stress equilibrium. The presented devices are expected to pave the way for practical use of solar-thermal energy harvesting.

I. INTRODUCTION

Optical absorbers based on nanostructures and electromagnetic (EM) metamaterials (MMs) have been considered as an indispensable optical component in diverse applications including sensing and spectroscopy for ultranarrow band absorbers,[1–3] thermophotovoltaics,[4] thermal-emitting devices,[5–7] and solar–thermal harvesting devices.[8–10] In the last few decades, MMs have attracted considerable attention with these special properties and unprecedented EM phenomena, such as negative effective permeability, cloaking behavior, and backward propagation,[11,12] which cannot be gathered from nature. MM absorbers have widely been investigated with a variety of artificial metatoms and characteristic of block transmission and have also been recognized to have many potential applications.[12–15] However, the development and practical application of MM absorbers are greatly limited due to their less lattice constant[16] and complex technological process and being easily interfered with environmental factors.[17] Most recently, planar nanostructures that can provide high-efficiency functionality in much smaller volumes have been focused on intensive investigations. In most of the absorber research studies, narrow-band absorbers play an important role in high sensitivity sensor systems based on Tamm surface plasmon structures[18] and special 2D materials, such as graphene and transition metal dichalcogenides (TMDCs),[19–22] while these narrowband absorbers are limited to extend photovoltaics (PV) and thermophotovoltaic applications.[23] Consequently, it is extremely necessary to develop the novel absorber scheme from narrowband to broadband absorption that can address the aforementioned limitations and promote the applications of solar-thermal energy simultaneously.

Most of the existing perfect planar absorbers exploit absorptive metals or semiconductors with optical thickness to block transmission and reduce reflection to achieve the desired unilateral and omnidirectional absorption characteristic.[24] Perhaps, it is a major obstacle to improving the efficiency of solar-thermal energy absorption. In addition, compared with the devices using non-flexible substrates, such as glass and ceramics, it is found that flexible devices have many very practical and unique features—light weight, conformal ability, suitable for mass production, and shipment.[25–28] It is noteworthy that the flexible substrates are highly vulnerable to strain and stress action of multilayers naturally owing to these extremely thin thicknesses, resulting in a significantly downgraded performance. To this regard, one of the solutions is to deposit a balanced film system on the other side of the substrate to counteract the compressive and tensile stresses. However, there is also a defect of limited adaptability to achieve complete stress balance for each layer, especially for thin metal layer. Therefore, sufficiently depositing the multilayer films with bilateral-symmetric structure is a prerequisite for its widespread applications.

Here, we propose two novel transversely symmetrical multilayer absorbers based on the antireflection (AR) coatings, the metal-insulator-metal (MIM) resonator, a substrate, MIM resonator and AR coatings (AMSMA) that could enable omnidirectional, ultrabroadband response with nearly perfect absorption and polarization-independence across the entire VIS and near-infrared (NIR) spectra. Among them, Cr is chosen as the bimetallic layers in the MIM structure and the graded refractive index dielectrics are exploited as the AR coatings to enhance transmission, which are explained in more detail in subsequent work. First, the optimum configuration with glass-substack is investigated using numerical simulations, and the design is fabricated and characterized. The proposed planar stack displays an average absorption of ~93% over the visible (VIS) and NIR range from 400 to 2500 nm and 98% in the VIS range. On the basis of saving metal greatly, the interaction of Cr layers at different locations can be fully utilized to achieve the ultrabroadband absorption effect to a large extent. Concurrently, angle-invariant performance can be maintained up to ±60° for Transverse-Electric (TE) and Transverse-Magnetic (TM) polarization waves from both bilateral illumination directions; thus, the proposed planar stack can equate to a spherical absorber. Furthermore, in order to potentially extend the viability of devices to various application fields over a large area, the flexible material PMMA with a modest high temperature resistance is involved for the structural substrate fabrication, which forms an important part of flexible absorption devices with bending deformation on the optical properties. The described concept holds great promise in a broad range of applications such as flexible electronics, optical lithography, and solar panels.

II. RESULTS AND DISCUSSIONS

Figure 1(a) shows a schematic diagram of the proposed ultrabroadband absorber that is made of a glass substrate and AM-MA multilayers, where SiO_2 (d_{s1}) and TiO_2 (d_t) with an refractive index gradient act as the AR layers and Cr (d_{c1}), SiO_2 (d_{s2}), and Cr (d_{c2}) as the MIM layers are deposited on top of the optically thick glass substrate. The bottom layers of the glass are symmetrically distributed with the upper films. The four Cr layers from the bottom up are defined as #1 to #4, respectively. To achieve high-efficiency broadband absorption behavior, the dimension parameters of the configuration can be analyzed theoretically by using the transfer matrix method (TMM) and optimized based on the optical film design tool—TFCalc. The thickness of each film is set as d_{s1} = 99 nm, d_t = 60 nm, d_{c1} = 7 nm, d_{s2} = 104 nm, and d_{c2} = 10 nm, and the thin glass substrate has a negligible effect on absorption characteristics. Considering the antireflection effect, the reflectance and transmission are greatly reduced by lossy metallic films so that our transversely symmetrical multilayer system can be seen as a perfect absorber under the TM and TE waves. An optical photograph of the fabricated sample is given in Fig. 1(b) which is totally black since the omnidirectional incidence in natural light is completely absorbed. Plotted in Fig. 1(c) are the simulated absorption spectra (blue lines) of the whole configuration over the full range, displaying an excellent agreement with measured inset illustration (orange line) in the VIS range. The proposed planar stack shows an average absorption of ~93% over the VIS and NIR range from 400 to 2500 nm in the simulation results and 98% in the VIS range. The device

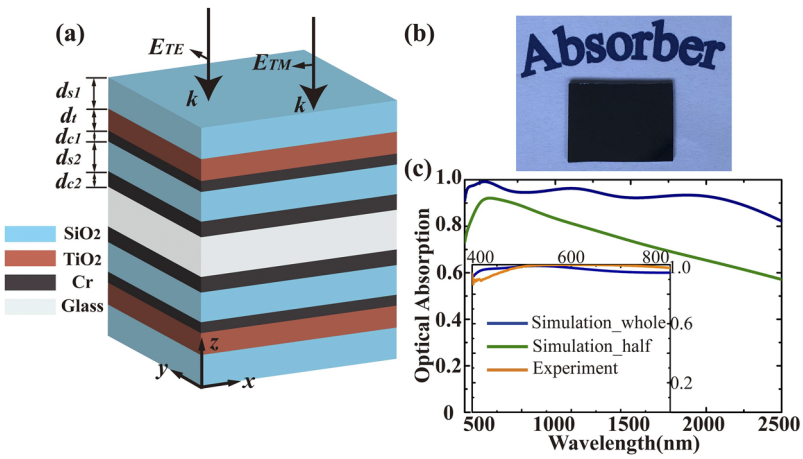

FIG. 1. (a) Schematic diagram of the proposed ultrabroadband visible-NIR absorber with a glass substrate. (b) Photo of the fabricated absorber on the glass substrate under normal incidence. (c) Simulated and measured absorption spectra for the full range and visible range. Simulation_whole and simulation_half represent the absorption of the whole structure and the structure on one side of the glass substrate, respectively.

fabrication is carried out using electron beam evaporation on the substrate, in which the Cr evaporation rate is 0.5 Å/s. The homemade spectral measurement setup with a fiber spectrophotometer (USB 2000+VIS-NIR-ES) is used to measure the VIS absorbance spectra. It is not necessary to consider the slight differences in partial segments because of the tiny change in the permittivity of Cr with chamber pressure, evaporation temperature, and rate, which can be neglected.[29] Moreover, in order to correspond to the characteristics and absorption contribution of Cr in each layer in the follow-up work and highlight the broadband and high-intensity absorption characteristics of the transversely symmetrical structure, we also simulated the absorption spectrum of the structure on the side of the glass substrate (green line). It can be seen that in the whole research wave band, the absorptivity decreases obviously and is weaker than that of the whole structure. Multiple resonances in each MIM stack at different absorptive ranges are established, and the broadband absorption range can reach more than 2 μm, which is far exceed other research, the metasurfaces and the stack absorbers.

To investigate the effect of the multiple resonances and top metallic layers, which involves the reasonable range of the refractive indices (both real and imaginary parts), as well as the determination of materials in different bands for outer metal layers (#1 and #4), several 3D contour plots are presented in Fig. 2. With this simulation, the permittivity values of intermediate double layer Cr (#2 and #3) and the optical constants of SiO_2 are obtained from the data of Palik, and the refractive index of TiO_2 is set as 2.3, in order for the broadband absorption to reach above 0.9, which means that the refractive indices of outer metal layers should stay inside the innermost circle of the horizontal contour. We can see from the contour analysis diagrams that the four wavelengths selected can basically cover the VIS to NIR bands what we concerned. Ordinarily, there are many metals, semiconductors, or their alloys that can be used as absorptive layers to achieve high-efficiency absorption, such as titanium (Ti), germanium (Ge), and nickel (Ni). In contrast to these cases, absorption was eventually identified using thin Cr to serve as the outer absorptive metal based on its optically lossy characteristics and weak dispersion, which can satisfy our research requirement. For simplicity, SiO_2 is used as the insulator layer in the MIM stack with the optimized thickness for its high transparency broadband window without dispersive optical nature over the full wavelength range.[30,31]

Figures 3(a) and 3(b) display normalized electric-field distribution and absorption profile, which as a function of incidence wavelength, into the proposed multilayer structural broadband absorbers. As can be seen from Fig. 3(a), it is apparent that there are several regions where the electric field is intensively focused on the top AR coatings over the full wave range and SiO_2 layers over the VIS range with different performance. The E-field is shown to be highly confined by double absorptive metals (#3 and #4) and trapped in the dielectric layers of the upper portion of the structure not only at resonance wavelength but across the entire investigated range with TM wave incidence. Obviously, the phenomenon can be easily considered by examining the frequency response of the MIM structure at various research areas. The simple Cr-SiO_2-Cr model resembles a Fabry-Perot-like (FP-like) nanocavity within a short wavelength range due to several lossy metallic boundaries outside of the cavity construction.[32] While the light intensity is localized to a greater extent above the upper layer of Cr (#4), the extinction coefficient increases gradually in the long-wave band.[33,34] The calculated full optical absorption diagram shown in Fig. 3(b) further unveils the reason for the contribution of thin Cr films at different positions as the optical absorption (P_{abs}) is directly proportional to the whole E-field intensity ($|E|^2$). It can be expressed as

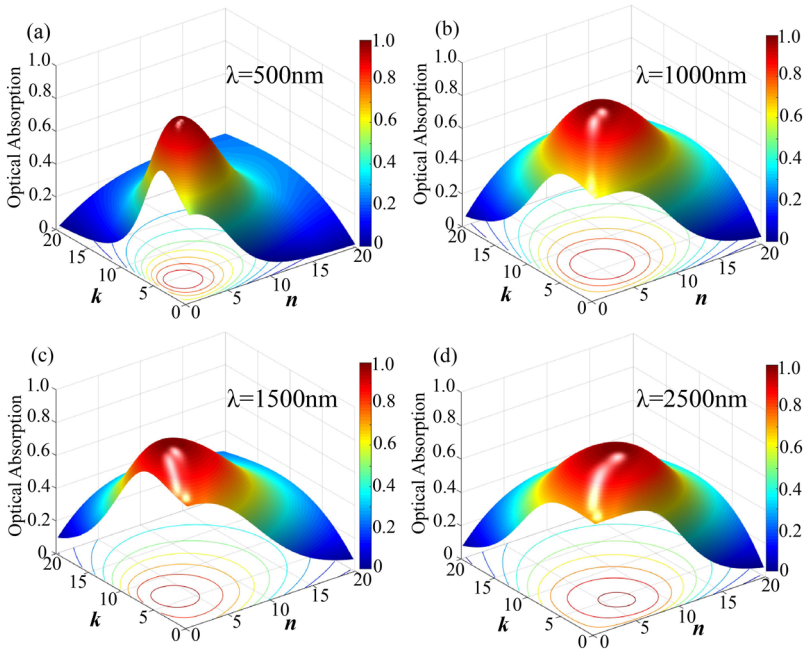

FIG. 2. The 3D contour plots of the absorber showing the optical absorption value at the wavelength of (a) 500 nm, (b) 1000 nm, (c) 1500 nm, (d) 2500 nm for #1 and #4 Cr layers as a function of real and imaginary parts.

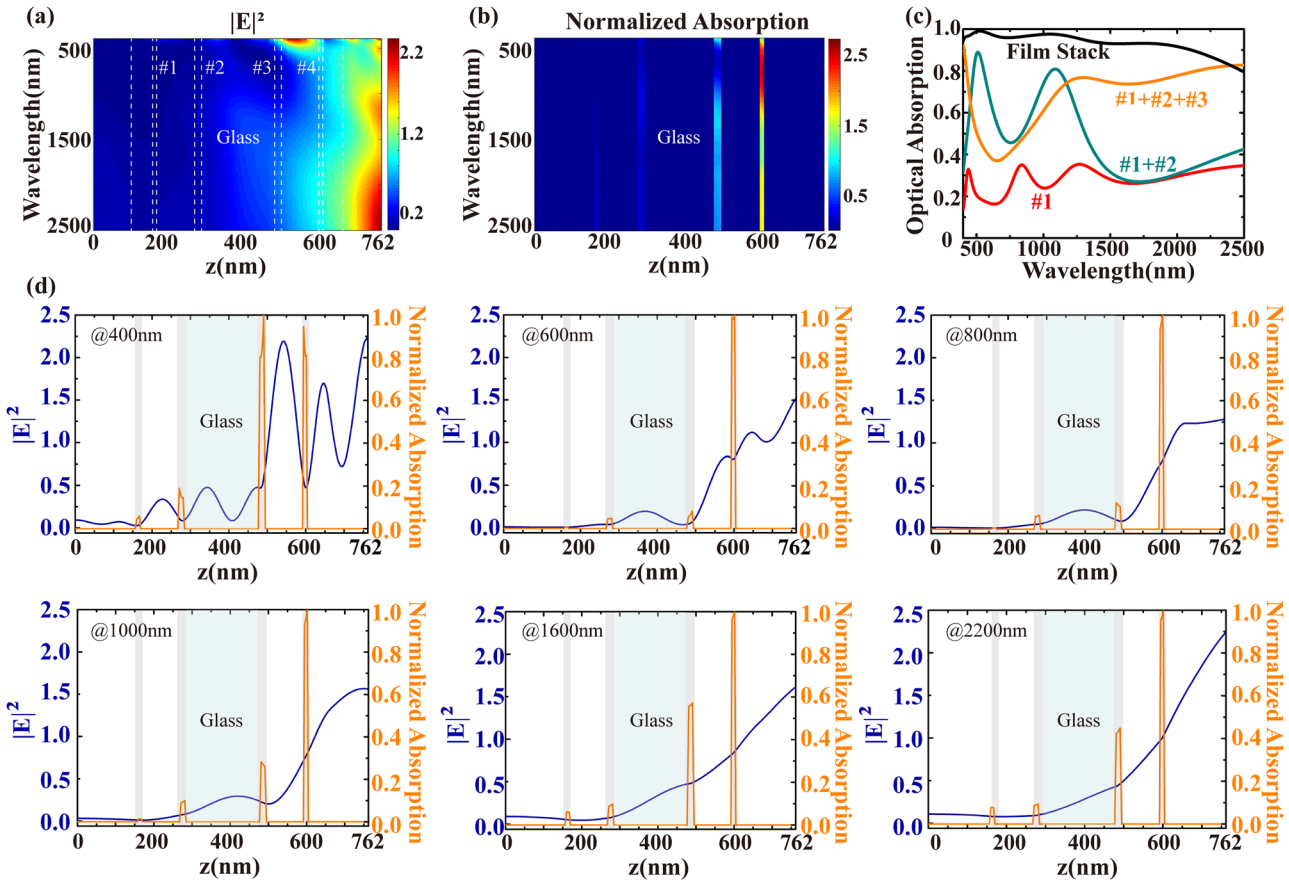

FIG. 3. (a) Electric field distribution within the whole structure at all wavelengths and (b) calculated full optical absorption diagram according to the electric field distribution. (c) Optical absorption spectrum corresponding to different layers of Cr; other layers are considered as nonabsorptive hypothetic materials. (d) The electric field distribution within the whole layers and normalized optical absorption with increasing wavelength.

$$P_{\text{abs}} = \frac{1}{2}\omega\varepsilon_0 nk|E|^2, \tag{1}$$

where ω is the angular frequency, ε_0 is the permittivity of free space, and n and k are the real and imaginary part of the refractive index.[23,35] In addition to the normal attenuation of light waves, four-layer Cr exhibits different physical performance, in which the absorption inside the top Cr films is probably wavelength sensitive. The electric field can only be considered as the traveling wave type because there are only ultrathin loss layers without a thick reflector.

On the basis of the descriptions containing the field intensity distribution in Fig. 3(a) and the absorptivity aimed for Cr in different layers in Fig. 3(b), the clustering physical principle of Cr thin films is further elaborated in Fig. 3(c), where the extinction coefficients of the unconsidered Cr layers are assumed to be zero, while the optical constants of other dielectrics remain invariant. For the red curve, only the bottom Cr (#1) layer plays an absorptive role, while the extinction coefficients of the other Cr layers are considered to be set as nonabsorptive hypothetic materials in the simulation of this section. Note that the absorption of the whole structure is significantly improved compared with the less Cr layer situation by adjusting the quantity of Cr layers. Simultaneously, the absorption of the full film stack is much higher than other cases, which corresponds to the phenomenon in Fig. 3(b). To better illustrate the relationship of the electromagnetic energy and absorption characteristics with the width of the absorber layer, the curves of $|E|^2$ and the normalized absorption based on the TMM along the z axis at different incidence wavelengths are shown in Fig. 3(d). We can see from the full range figures that the E-field intensity $|E|^2$ in Cr is less than that in SiO_2 in the short wavelength range. In contrast to these cases, with the increase in wavelength, $|E|^2$ shows an exponential decay trend. According to the propagation characteristics of the electromagnetic wave between interfaces toward the shorter wavelength regime, the E-field is continuous in the tangential direction of the interface, while a mutation occurs in the normal direction, which makes $|E_{n2}| \neq |E_{n1}|$. Furthermore, if $\varepsilon_1 > \varepsilon_2$, $|E_{n2}| > |E_{n1}|$. Thus, when the electromagnetic wave enters Cr from SiO_2, $|E|^2$ in the Cr is always less than that in SiO_2 because $\varepsilon_{Cr} > \varepsilon_{SiO2}$, which is consistent with the simulation results. However, for the long wavelength incidence, the wavelength is much larger than the thickness of Cr, indicating that the influence of Cr on electromagnetic field propagation is almost negligible, which is equivalent to

the propagation of electromagnetic wave in a uniform attenuation medium, thus showing an exponential attenuation curve.

Effects of each coating layer on the optical performance of the absorber are studied by using an optical admittance figure that is a graphical technique showing the progression in the surface admittance through the full configuration from the symmetrical bottom material to the incident dielectric. The optical admittance Y can be expressed initially as Y = H/E, where H and E mean the magnetic-field and the electric-field intensity, respectively. For a three-layer system, we first investigate the absorptance of the research film (n_1) on a substrate (n_2); the phase factor can be defined as[36]

$$\delta_1 = \frac{2\pi n_1 d \cos\theta_1}{\lambda}, \tag{2}$$

where d denotes the thickness of the research film, θ_1 denotes the incident angle, and λ denotes the incident wavelength. In the TMM form,

$$\begin{bmatrix} E_1 \\ H_1 \end{bmatrix} = \begin{bmatrix} \cos\delta_1 & \frac{i\sin\delta_1}{n_1} \\ in_1\sin\delta_1 & \cos\delta_1 \end{bmatrix} \begin{bmatrix} E_2 \\ H_2 \end{bmatrix}. \tag{3}$$

Consequently, the optical admittance Y of a multilayer system can be simply expressed as

$$Y = \begin{bmatrix} E_1 \\ H_1 \end{bmatrix} = \begin{bmatrix} B \\ C \end{bmatrix} = \begin{bmatrix} \cos\delta_1 & \frac{i\sin\delta_1}{n_1} \\ in_1\sin\delta_1 & \cos\delta_1 \end{bmatrix} \begin{bmatrix} 1 \\ n_2 \end{bmatrix}. \tag{4}$$

With this equivalent admittance, determining the optical absorptance of our proposed structure with symmetrical film distribution is similar to the three-layer system situation. Thus, the total characteristic matrix should be calculated as the superposition of several characteristic matrices for each film,

$$\begin{bmatrix} B \\ C \end{bmatrix} = \prod_{j=1}^{a} \begin{bmatrix} \cos\delta_1 & \frac{i\sin\delta_1}{n_1} \\ in_1\sin\delta_1 & \cos\delta_1 \end{bmatrix} \begin{bmatrix} 1 \\ n_{sub} \end{bmatrix}. \tag{5}$$

Moreover, the reflectance can be obtained based on the Fresnel reflection formula,

$$R = |r|^2 = \left(\frac{Y_1 - Y_2}{Y_1 + Y_2}\right)\left(\frac{Y_1 - Y_2}{Y_1 + Y_2}\right)^*, \tag{6}$$

where Y_1 and Y_2 denote the admittance of the incident dielectric and the termination dot of the total film stack.

Figure 4(a) uses the same medium parameter setting method as Fig. 3(c) and verifies that with the increase in the quantity of Cr layers in operation, the terminal point (orange dot) of admittance is finally closer to (1, 0), i.e., the index of the incident medium, air. We also note that reflectance marked in the figure is reduced gradually, and the perfect absorption is finally achieved at 2000 nm incidence by the entire film stack. Figure 4(b) presents the optical admittances of the entire configuration as the thicknesses of the each film increase. From the comparison results of admittance loci at different wavelengths, MIM resonance structure has the largest effective admittance, and it is noteworthy that the contribution of effective admittance of Cr in a short-wave band is much higher than that in a long-wave band.[37]

Previous descriptions of this work focus on the effects of TM waves on the proposed absorber. Next, we also simulated the

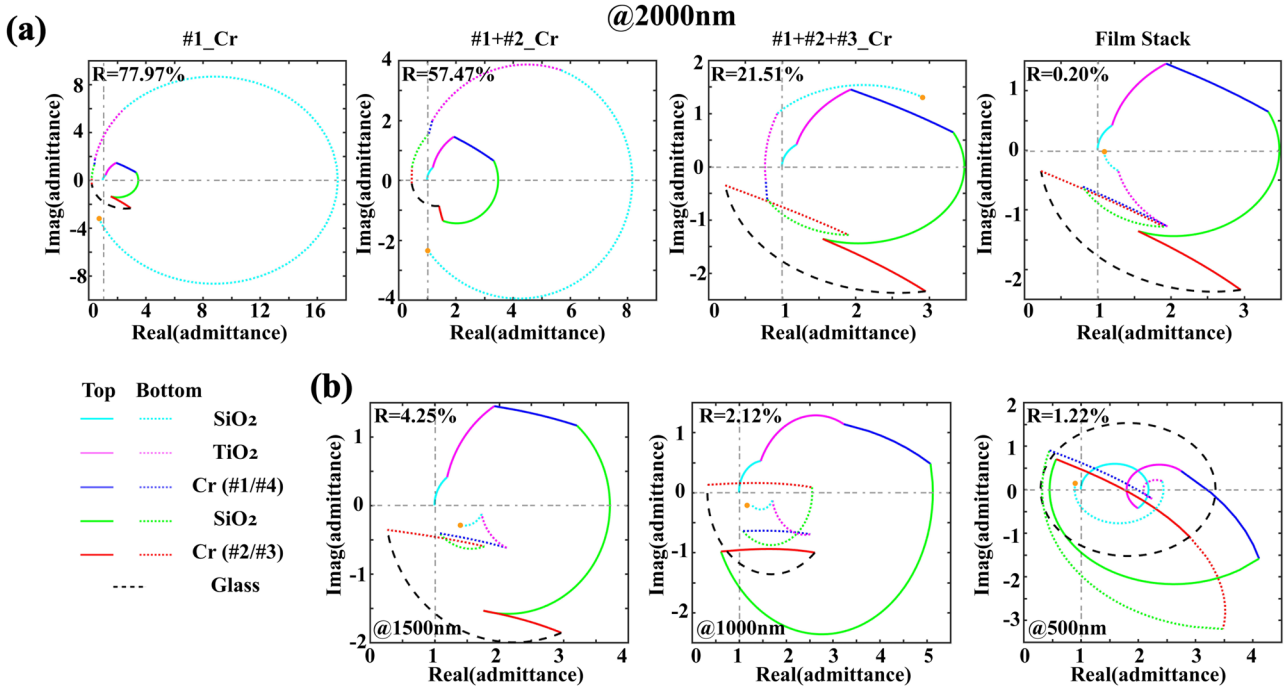

FIG. 4. (a) Optical admittance diagrams of the entire structure corresponding to different layers of Cr at λ = 2000 nm; other layers are considered as absorptive hypothetic materials. (b) Optical admittance loci at different wavelengths. The reflectance marked in the figure is calculated by the Fresnel reflection formula with the terminal admittance.

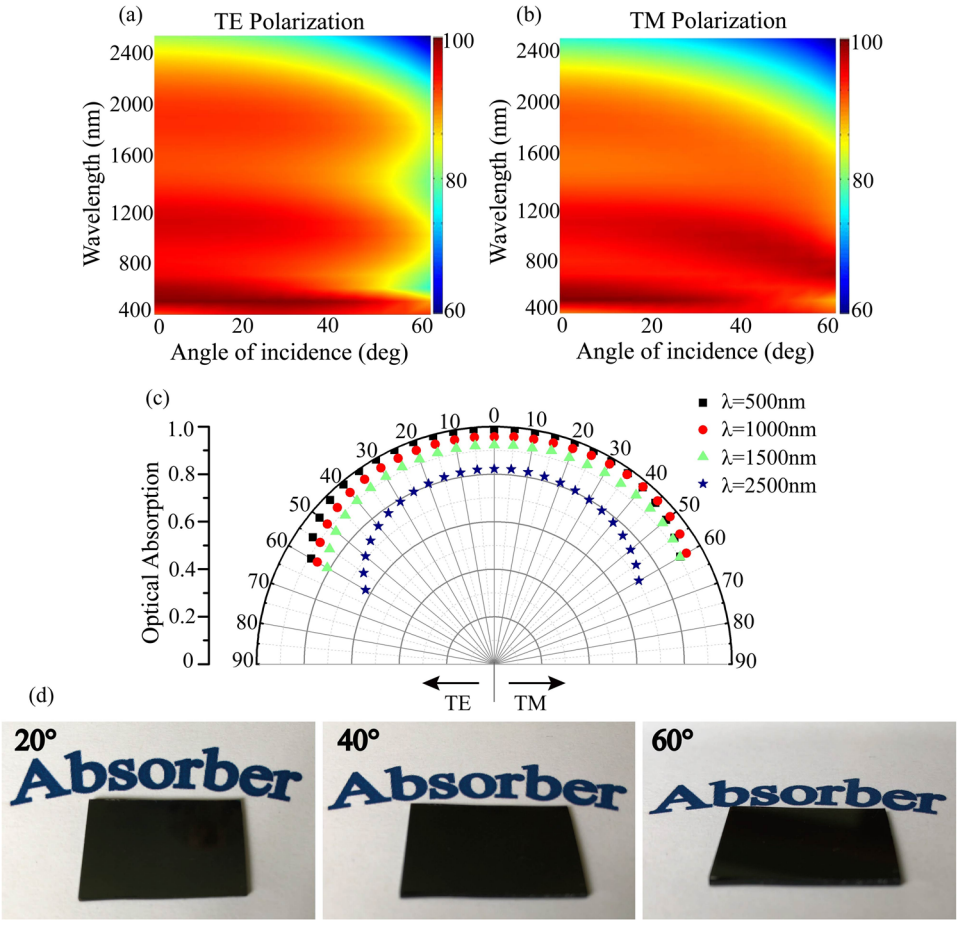

FIG. 5. Simulated incident angle θ resolved absorption spectra for (a) TE and (b) TM polarization waves. (c) Simulated directional absorptance as a function of θ at different wavelengths. (d) Optical images of the fabricated absorber acquired at different incident angles.

angular-dependence absorption spectra for TE and TM polarization waves, as shown in Figs. 5(a)–5(c). A highly efficient absorption performance encompassing the wavelengths from VIS to NIR is accomplished over a broad range of incident angles up to ±60°. In individual extreme cases, to clearly see that for TE, with long-band large-angle incidence, and for TM, with short-band large-angle incidence, the average absorption efficiency can still reach higher than 93%. Figure 5(d) exhibits photographs of the fabricated black absorbers taken at three different observing angles within indoor ambient illumination, showing an angle-polarization invariant even at large incident angles. On the basis of interaction between the gradient index AR coating layers and strong resonance effects of the MIM structure, the phase invalidation response between dielectrics and metal films interfaces is conducive to the angle-insensitivity performance.[38,39]

In order to expand the wide application of absorbers in high ductility solar-thermal energy collectors, ultrabroadband absorbers based on flexible substrates were investigated. As the fabrication of the proposed structure just involves an uncomplicated evaporation process, the multilayer devices can be easily implemented on a flexible platform. Figure 6(a) shows a schematic diagram of the flexible absorber, in which the substrate is replaced by PMMA, and the rest is consistent with the composition of the planar absorber. The optical image of the fabricated flexible structural absorber is provided in Fig. 6(b). PMMA is chosen owing to its weak dispersion, similar refractive index to glass, high transmittance in the research band, and basically stable spectral characteristics. Subsequent work will show that the absorptivity can be maintained at a stable high efficiency at the same time of large deformation. As shown in Fig. 6(c), in comparison with previous planar absorbers, there is only a slight difference in the perfect absorption performance between the two structures. The main reason is that the selected PMMA sample material is a little bit thicker than glass and slightly different in the equivalence of transmission characteristics. Furthermore, considered that the thermal stability of flexible materials is weakened during vacuum evaporation, which affects the quality of films, the fabrication of them should strictly control the experimental indexes. From the inset of Fig. 6(c), it can be concluded that the absorption of the fabricated sample in the VIS band is roughly equal to that of the simulation.

To further explore the absorption performance of flexible devices, a bending coefficient is defined as B = t/s, where t and s denote the bending height and bending span of rectangular (aspect ratio = 5:3) absorber samples, respectively, and the schematic

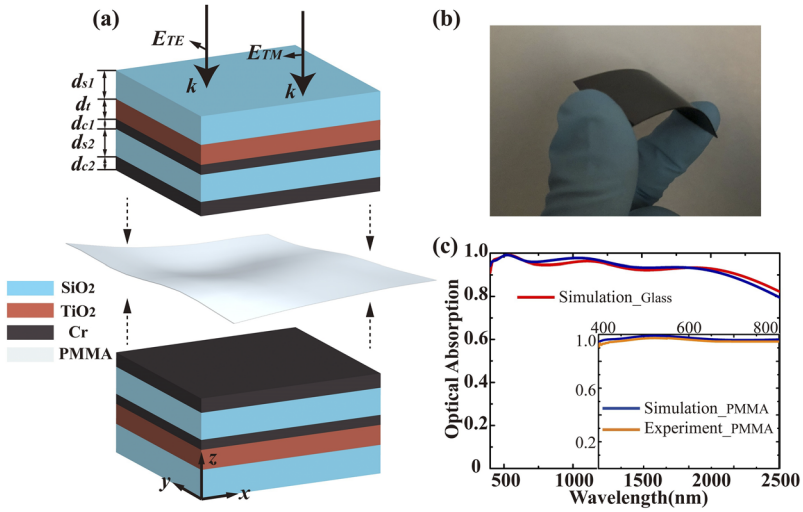

FIG. 6. (a) Schematic diagram of the proposed ultrabroadband and flexible visible-NIR absorber with a PMMA substrate. (b) Photo of the fabricated flexible absorber under normal incidence. (c) Simulated and measured absorption spectra for the 400–2500 nm and visible range.

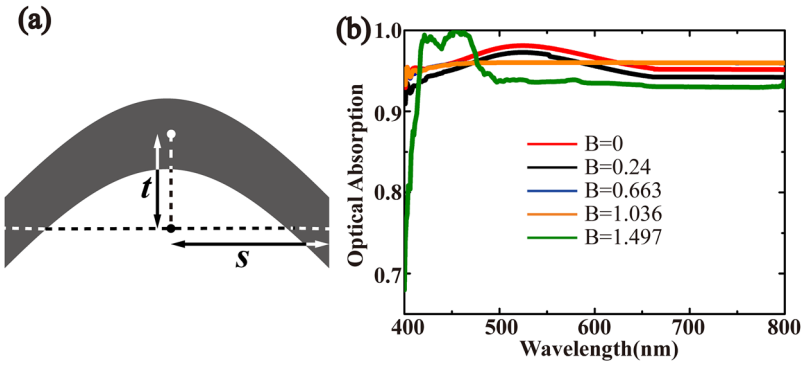

FIG. 7. (a) Schematic diagram of the bending flexible absorber. (b) Measured bending coefficient (B = t/s) of the proposed flexible absorber at different deforming degrees.

diagram is shown in Fig. 7(a). From Fig. 7(b), it is apparent that the B is less than 1.497, that is, when the curvature of the half-edge absorber is about 70°, the absorption characteristics are almost unchanged, which can satisfy the near-perfect absorption effect under the normal incidence condition.

III. CONCLUSION

In summary, two high-efficiency and ultrabroadband multilayer absorbers based on the transversely symmetrical planar and flexible structure have been demonstrated. The proposed planar and flexible devices present the average absorption of ~93% over the visible (VIS) and near-infrared (NIR) range from 400 to 2500 nm and 98% in the VIS range. The greater angular-dependence can be simulated up to ±60°. The designed flexible device is simply composed of the AM-MA structure and PMMA substrate, which can perform nearly perfect absorption in the case of high bending. Both the double MIM resonator of the multilayer stack comprising economic absorptive materials and the AR property arising from the graded index profile structure contribute to the ultrabroadband absorption with high-efficiency of these planar and flexible devices. The ultrathin symmetrical structure can significantly improve the bilateral absorption performance and is expected to play a more valuable role in various applications such as solar-thermal collectors, bolometers, and photodetection.

ACKNOWLEDGMENTS

This work was supported by the National Natural Science Foundation of China (Grant Nos. 11504139, 11504140, and 11811530052), the China Postdoctoral Science Foundation (Grant Nos. 2017M611693 and 2018T110440), the Intergovernmental Science and Technology Regular Meeting Exchange Project of the Ministry of Science and Technology of China (Grant No. CB02-20), and the National Science Foundation (Grant Nos. CMMI-1405078, CMMI-1554189, and CMMI-1634832).

REFERENCES

[1]Z. Y. Fang, Y. M. Wang, A. E. Schlather, Z. Liu, P. M. Ajayan, F. J. G. de Abajo, P. Nordlander, X. Zhu, and N. J. Halas, "Active tunable absorption enhancement with graphene nanodisk arrays," Nano Lett. **14**(1), 299–304 (2014).
[2]X. Lu, R. Wan, and T. Zhang, "Metal-dielectric-metal based narrow band absorber for sensing applications," Opt. Express **23**(23), 29842 (2015).
[3]D. Wu, R. F. Li, Y. M. Liu, Z. Y. Yu, L. Yu, L. Chen, C. Liu, R. Ma, and H. Ye, "Ultra-narrow band perfect absorber and its application as plasmonic sensor in the visible region," Nanoscale Res. Lett. **12**(1), 427 (2017).

[4]K. Aydin, V. E. Ferry, R. M. Briggs, and H. A. Atwater, "Broadband polarization-independent resonant light absorption using ultrathin plasmonic super absorbers," Nat. Commun. **2**(1), 517 (2011).
[5]N. I. Landy, C. M. Bingham, T. Tyler, N. Jokerst, D. R. Smith, and W. J. Padilla, "Design, theory, and measurement of a polarization-insensitive absorber for terahertz imaging," Phys. Rev. B **79**(12), 125104 (2009).
[6]N. Liu, M. Mesch, T. Weiss, M. Hentschel, and H. Giessen, "Infrared perfect absorber and its application as plasmonic sensor," Nano Lett. **10**(7), 2342–2348 (2010).
[7]W. Streyer, S. Law, G. Rooney, T. Jacobs, and D. Wasserman, "Strong absorption and selective emission from engineered metals with dielectric coatings," Opt. Express **21**(7), 9113–9122 (2013).
[8]P. Li, B. Liu, Y. Ni, K. K. Liew, J. Sze, S. Chen, and S. Shen, "Large-scale nanophotonic solar selective absorbers for high efficiency solar thermal energy conversion," Adv. Mater. **27**(31), 4585–4591 (2015).
[9]C. Y. Yang, C. G. Ji, W. D. Shen, K. T. Lee, Y. G. Zhang, X. Liu, and L. J. Guo, "Compact multilayer film structures for ultrabroadband, omnidirectional, and efficient absorption," ACS Photonics **3**(4), 590–596 (2016).
[10]Q. Liang, T. Wang, Z. Lu, Q. Sun, Y. Fu, and W. Yu, "Metamaterial-based two dimensional plasmonic subwavelength structures offer the broadest waveband light harvesting," Adv. Opt. Mater. **1**(1), 43–49 (2013).
[11]D. R. Smith, W. J. Padilla, D. C. Vier, S. C. Nemat-Nasser, and S. Schultz, "Composite medium with simultaneously negative permeability and permittivity," Phys. Rev. Lett. **84**(18), 4184–4187 (2000).
[12]D. Schuri, J. J. Mock, B. J. Justice, S. A. Cummer, J. B. Pendry, A. F. Starr, and D. R. Smith, "Metamaterial electromagnetic cloak at microwave frequencies," Science **314**(5801), 977–980 (2006).
[13]S. L. Wu, Y. Gu, Y. Ye, H. Ye, and L. S. Chen, "Omnidirectional broadband metasurface absorber operating in visible to near-infrared regime," Opt. Express **26**(17), 21479 (2018).
[14]X. Huang, W. He, F. Yang, J. Ran, B. Gao, and W. L. Zhang, "Polarization–independent and angle-insensitive broadband absorber with a target-patterned graphene layer in the terahertz regime," Opt. Express **26**(20), 25558–25566 (2018).
[15]N. Mou, S. Sun, H. Dong, S. Dong, Q. He, L. Zhou, and L. Zhang, "Hybridization-induced broadband terahertz wave absorption with graphene metasurfaces," Opt. Express **26**(9), 11728–11736 (2018).
[16]Y. J. Yoo, H. Y. Zheng, Y. J. Kim, J. Y. Rhee, J. H. Kang, K. W. Kim, H. Cheong, Y. H. Kim, and Y. P. Lee, "Flexible and elastic metamaterial absorber for low frequency, based on small-size unit cell," Appl. Phys. Lett. **105**(4), 041902 (2014).
[17]L. Huang, D. R. Chowdhury, S. Ramani, M. T. Reiten, S. N. Luo, A. K. Azad, A. J. Taylor, and H. T. Chen, "Impact of resonator geometry and its coupling with ground plane on ultrathin metamaterial perfect absorbers," Appl. Phys. Lett. **101**(10), 101102 (2012).
[18]X. Wang, X. Jiang, Q. You, J. Guo, X. Dai, and Y. Xiang, "Tunable and multichannel terahertz perfect absorber due to Tamm surface plasmons with graphene," Photonics Res. **5**(6), 536–542 (2017).
[19]Q. Yang, C. Zhang, S. Wu, S. Li, Q. Bao, and V. Giannini, "Photonic surface waves enabled perfect infrared absorption by monolayer graphene," Nano Energy **48**, 161–169 (2018).
[20]K. Li, J. M. Fitzgerald, and X. F. Xiao, "Graphene plasmon cavities made with silicon carbide," ACS Omega **2**, 3640–3646 (2017).
[21]X. Xu, N. M. Gabor, J. S. Alden, A. M. Van der Zande, and P. L. Mceuen, "Photothermoelectric effect at a graphene interface junction," Nano Lett., **10**(2), 562–566 (2010).
[22]X. Wang, J. Wang, Z. D. Hu, T. Sang, and Y. Feng, "Perfect absorption of modified-molybdenum-disulfide-based Tamm plasmonic structures," Appl. Phys. Express **11**(6), 062601 (2018).
[23]K. T. Lee, C. Ji, and L. J. Guo, "Wide-angle, polarization-independent ultrathin broadband visible absorbers," Appl. Phys. Lett. **108**(3), 031107 (2016).
[24]L. Qin, S. Wu, C. Zhang, and X. Li, "Narrowband and full-angle refractive index sensor based on a planar multilayer structure," IEEE Sens. J. **19**, 2924–2930 (2019).
[25]J. L. Wang, B. Z. Zhang, X. Wang, and J. P. Duan, "Flexible dual-band band-top metamaterials filter for the terahertz region," Opt. Mater. Express **7**(5), 1656–1665 (2017).
[26]H. Tao, C. M. Bingham, A. C. Strikwerda, D. Pilon, D. Shrekenhamer, N. I. Landy, K. Fan, X. Zhang, W. J. Padilla, and R. D. Averitt, "Highly flexible wide angle of incidence terahertz metamaterial absorber," Phys. Rev. B **78**(24), 241103 (2008).
[27]D. H. Kim, D. S. Kim, S. Hwang, and J. H. Jang, "Surface relief structures for a flexible broadband terahertz absorber," Opt. Express **20**(15), 16815–16822 (2012).
[28]K. T. Lee, S. Y. Han, and H. J. Park, "Omnidirectional flexible transmissive structural colors with high-color-purity and high-efficiency exploiting multicavity resonances," Adv. Opt. Mater. **5**(14), 1700284 (2017).
[29]K. T. Lee, J. Y. Lee, S. Seo, and L. J. Guo, "Colored ultrathin hybrid photovoltaics with high quantum efficiency," Light: Sci. Appl. **3**(10), e215 (2014).
[30]B. Zhang, Y. Zhao, Q. Hao, B. Kiraly, I. C. Khoo, S. Chen, and T. J. Huang, "Polarization-independent dual-band infrared perfect absorber based on a metal-dielectric-metal elliptical nanodisk array," Opt. Express **19**(16), 15221–15228 (2011).
[31]J. Park, J. H. Kang, A. P. Vasudev, D. T. Schoen, H. Kim, and E. Hasman, "Omnidirectional near-unity absorption in an ultrathin planar semiconductor layer on a metal substrate," ACS Photonics **1**(9), 812–821 (2014).
[32]S. A. Dereshgi, A. Ghobadi, H. Hajian, B. Butun, and E. Ozbay, "Ultra-broadband, lithography-free, and large-scale compatible perfect absorbers: The optimum choice of metal layers in metal-insulator multilayer stacks," Sci. Rep. **7**(1), 14872 (2017).
[33]Z. Li, E. Palacios, S. Butun, H. Kocer, and K. Aydin, "Omnidirectional, broadband light absorption using large-area, ultrathin lossy metallic film coatings," Sci. Rep. **5**, 15137 (2015).
[34]M. A. Kats, R. Blanchard, P. Genevet, and F. Capasso, "Nanometre optical coatings based on strong interference effects in highly absorbing media," Nat. Mater. **12**(1), 20–24 (2012).
[35]H. Kocer, S. Butun, Z. Li, and K. Aydin, "Reduced near-infrared absorption using ultra-thin lossy metals in Fabry-Perot cavities," Sci. Rep. **5**, 8157 (2015).
[36]C. W. Lin, K. P. Chen, M. C. Su, T. C. Hsiao, S. S. Lee, and S. Lin, "Admittance loci design method for multilayer surface plasmon resonance devices," Sens. Actuators, B, **117**(1), 219–229 (2006).
[37]Y. J. Jen, W. C. Liu, T. K. Chen, S. W. Lin, and Y. C. Jhang, "Design and deposition of a metal-like and admittance-matching metamaterial as an ultra-thin perfect absorber," Sci. Rep. **7**(1), 3076 (2017).
[38]C. W. Cheng, M. N. Abbas, C. W. Chiu, K. T. Lai, M. H. Shih, and Y. C. Chang, "Wide-angle polarization independent infrared broadband absorbers based on metallic multi-sized disk arrays," Opt. Express **20**(9), 10376–10381 (2012).
[39]J. Y. Lee, K. T. Lee, S. Seo, and L. J. Guo, "Decorative power generating panels creating angle insensitive transmissive colors," Sci. Rep. **4**, 4192 (2014).